



Trans. Nonferrous Met. Soc. China 32(2022) 1460-1471

Transactions of Nonferrous Metals Society of China

www.tnmsc.cn



Simultaneous improvement of strength and ductility by Mn addition in extruded Mg-Gd-Zn alloy

Jun ZHAO¹, Bin JIANG², Yan SONG², Zuo-cai DAI¹, Li-wei LU³, Chao HE², Guang-sheng HUANG², Ding-fei ZHANG², Fu-sheng PAN²

- 1. School of Mechanical and Electrical Engineering, Hunan City University, Yiyang 413002, China;
- State Key Laboratory of Mechanical Transmissions, College of Materials Science and Engineering, Chongqing University, Chongqing 400044, China;

3. College of Materials Science and Engineering, Hunan University of Science and Technology, Xiangtan 411201, China

Received 19 April 2021; accepted 9 December 2021

Abstract: The influence of Mn content on the microstructure, tensile properties and strain-hardening behaviors of extruded Mg-1Gd-0.5Zn-xMn (x=0, 0.3 and 1, wt.%) alloy sheets was investigated by X-ray diffraction (XRD), scanning electron microscope (SEM), and electron backscatter diffraction (EBSD). The results show that the completely recrystallized grain structure and the extrusion direction (ED)-titling texture are observed in all the extruded sheets. The mean grain size and weakened ED-titling texture of the extruded sheets are gradually reduced with increasing Mn content. This is primarily associated with the formation of new fine α -Mn particles by Mn addition. Tensile properties show that the addition of Mn also leads to the improvement of yield strengths, ultimate tensile strengths and elongations of the extruded Mg-1Gd-0.5Zn-xMn sheets, which is mainly due to the fine grains and α -Mn particles. In addition, the Mg-1Gd-0.5Zn-1Mn sheet has the lowest strain-hardening exponent and the best hardening capacity among all prepared Mg-1Gd-0.5Zn-xMn sheets.

Key words: Mg-Gd-Zn alloy; Mn addition; microstructure; mechanical properties

1 Introduction

Magnesium alloys are potentially lightweight structures due to their brilliant characters, such as high specific strength and satisfactory electromagnetic shielding property. They are applied in the transportation and aerospace fields [1–3]. Achieving high-performance Mg alloys is an imperious demand for their broad application. Thermomechanical processing such as extrusion [4] and rolling [5,6] has been widely used as a practical approach to enhance the mechanical properties of Mg alloys. Unfortunately, the intense basal texture

of Mg alloys through extrusion or rolling is a primary factor to deteriorate the room temperature (RT) ductility and formability [7,8].

Recently, wrought Mg-Al-Zn and Mg-Sn-Zn based systems exhibit higher strength and ductility at RT [9-12]. For example, SHI et al [9] reported that a rolled Mg-2.5Zn-2Al (wt.%) sheet with 2 wt.% and 4 wt.% Sn additions exhibited good strength and ductility. Some studies have pointed out that Cu [10], Al [11] and Ca [12] additions effectively weakened the texture and reduced the grain size of the Mg-Sn-Zn based alloys, leading to the improved mechanical properties. Indeed, the ductility and strength of the Mg-7Sn-1Zn-4Al

alloy are ~17.7% and ~221 MPa, respectively [11]. In addition, Mg-Gd-Zn based alloys have recently drawn considerable attention because of their excellent strength and stretch formability. It has been proposed that Gd element has superior influence on the solid solution and ageing Furthermore, strengthening [13,14]. previous studies have reported that the additions of Ca, Zr, Ce and Al-Sr alloy increased the strengths of Mg-Gd-Zn based alloys [15-18]. FU et al [15] investigated a new cast Mg-3Gd-1Zn-0.3Zr (at.%) (GZ31-0.3Zr) alloy with a yield strength of 262 MPa after ageing. BIAN et al [16] pointed out that an Mg-14.02Gd-2.33Zn alloy with 0.6 wt.% Al-Sr master alloy exhibited high strength and ductility. WEN et al [17] revealed that the addition of Ca was helpful to the improvement of mechanical properties for the Mg-2Gd-4Zn alloys. Also, Mn is added to Mg alloys to discuss the effect of Mn on the microstructures and tensile properties [19-22]. Mn could purify iron and inclusion impurity during casting and act as a refiner (Mn particles) to hinder the grain growth during recrystallization [20]. KHAN et al [21] reported that Mn addition effectively reduced the grain size of the extruded AZ61 alloy, contributing to the improvement of tensile strength and fatigue life. LI et al [22] certified that Mn addition had no grain refining effect for the cast Mg-5.5Al-3Ca (wt.%) alloy, but it could expressively enhance the yield strength of the extruded alloy. Besides, WANG et al [23] explored the effect of Mn content on the microstructure and tensile properties of Mg-15Gd-1Zn (wt.%) alloy. Mn addition can lead to the formation of many small α -Mn particles and then improve the RT tensile properties of solutiontreated Mg-15Gd-1Zn-0.8 (wt.%) alloy. A yield strength of 154 MPa and an elongation of 7.4% were obtained for a solution-treated Mg-15Gd-1Zn-0.8Mn alloy. However, as mentioned above, many studies concentrate on the microstructure and tensile properties of Mg-Gd-Zn based alloys having high Gd addition. There is less report about the effect of Mn on the microstructure and tensile properties of Mg-Gd-Zn alloys having low Gd addition.

Thus, three Mg-1Gd-0.5Zn-xMn alloy sheets are obtained in the current work. It is hoped to investigate the effect of Mn contents on the microstructures and tensile properties of the

extruded Mg-1Gd-0.5Zn-xMn alloys. The presented results and discussion will provide an important basis to develop low-content high-performance Mg-RE alloys.

2 Experimental

Three alloys (Mg-1Gd-0.5Zn, Mg-1Gd-0.5Zn-0.3Mn and Mg-1Gd-0.5Zn-1Mn) using Mg (99.9%), Zn (99.6%), Mg-30Gd and Mg-15Mn master alloy (wt.%) were prepared in an induction furnace under protection CO₂ (99%) + SF₆ (1%) atmosphere followed by cast into a cylindrical iron mold. Chemical composition of cast alloys was determined by an X-ray fluorescence analyzer, as given in Table 1. Three Mg-Gd-Zn-Mn alloys are hereafter named as the GZ10, GZM100 and GZM101 alloys, respectively. The cast ingot was homogenized at 520 °C for 15 h and machined into the round rods with 80 mm in diameter and 60 mm in height. The homogenized ingot was extruded using a horizontal extrusion machine (XJ-500, China) at 400 °C. The extrusion speed and ratio were 1.5 m/min and 33:1, respectively. The extruded sheet with 56 mm in width and 3 mm in thickness was obtained.

Table 1 Chemical composition of studied alloys (wt.%)

Alloy	Mg	Gd	Zn	Mn
GZ10	Bal.	1.06	0.41	_
GZM100	Bal.	1.12	0.52	0.26
GZM101	Bal.	1.18	0.48	0.81

Tensile specimens with a gauge length of 12 mm, width of 6 mm and thickness of 3 mm were cut from the extruded sheets along the extrusion direction (ED) and transverse direction (TD). The tensile properties were tested by a CMT5105 machine at a constant speed of 1.5 mm/min. Identifying different phases in the extruded sheets were carried out using an X-ray diffraction (XRD) analysis. All specimens for the microstructural observation were taken from the normal direction (ND)-ED plane of the extruded sheets. Scanning electron microscopy (Tescan Vega 2 LMH) with an energy-dispersive spectrometer (EDS), electron back-scattered diffraction (JEOL JSM-7800F, EBSD) and transmission electron microscopy (Tecnai G2 F20), were utilized to characterize the

microstructure characterization. The step size, working distance and voltage for EBSD measurement were $0.8\,\mu m$, $15\,m$ m and $25\,k$ V, respectively. The accelerating voltages for SEM and TEM measurements were 15 and $200\,k$ V, respectively. EBSD data were examined using Channel five software. Thin foils for TEM observations are prepared by polishing (less than $40\,\mu m$) followed by an ion polishing system (GATAN691) operated at an accelerating voltage of $5.5\,k$ V and incident angle of 6° .

3 Results

3.1 Microstructure

Figure 1 shows the XRD patterns of extruded GZ10–xMn alloy sheets. The GZ10 sheet presents two phases: α-Mg and Mg₅Gd. Mn-containing sheets are composed of three phases: α-Mg, α-Mn and Mg₅Gd. The peak intensities of Mn phases increase with the increase of Mn content. Figure 2 shows the BSE micrographs of the extruded GZ10–xMn sheets and the EDS results of phase particles are listed in Table 2. Apparently, there exist some white particles randomly dispersed in the three samples. According to the EDS results, these particles are identified as the Mg₅Gd phase. However, due to the limited SEM detection, Mn-containing particles are not observed in the GZM100 and GZM101 sheets.

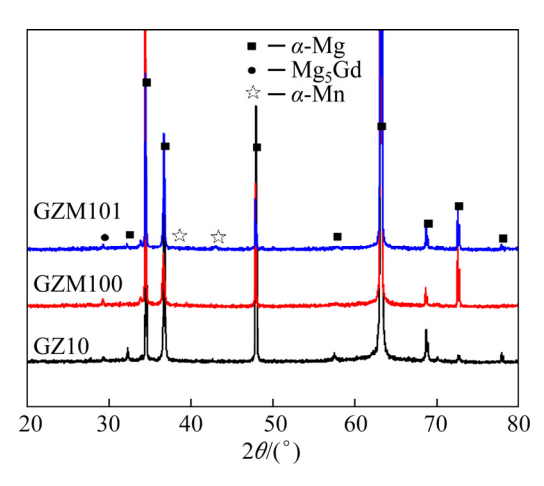


Fig. 1 XRD patterns of extruded sheets

To reveal further information about the distribution of phase particles, TEM images of the GZ10 and GZM101 sheets are demonstrated in Fig. 3. Only a few particles are observed in the GZ10 sheet and they are determined as Mg₅Gd

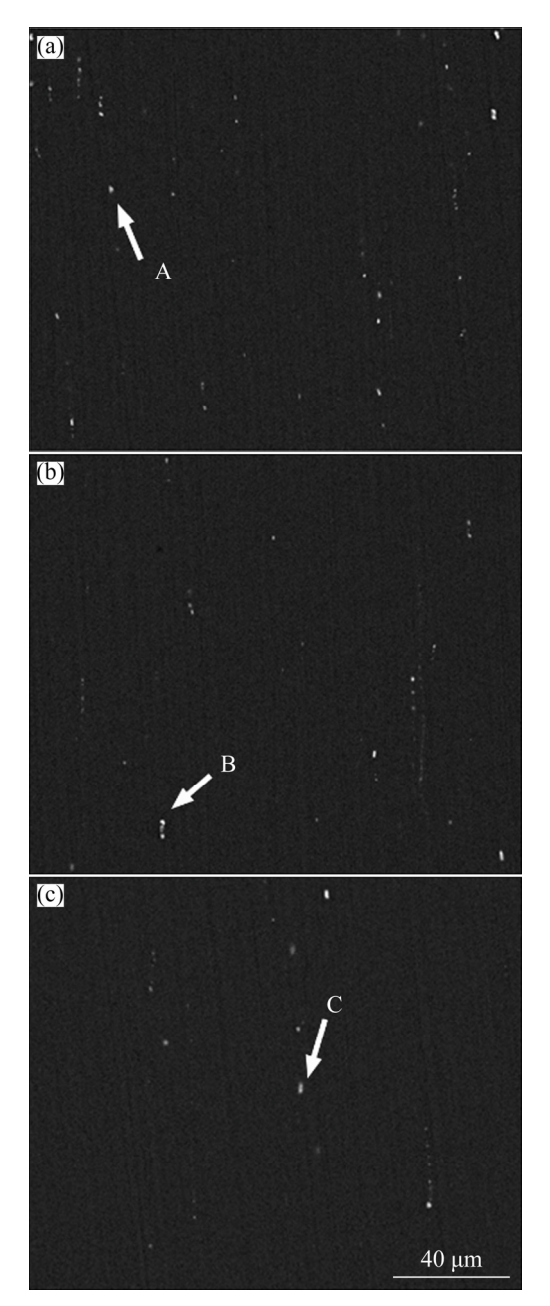


Fig. 2 SEM images of extruded GZ10 (a), GZM100 (b) and GZM101 (c) sheets

Table 2 EDS results of corresponding particles indicated in Fig. 2 (at.%)

Alloy	Position	Mg	Gd	Zn
GZ10	A	86.5	13.5	_
GZM100	В	82.8	17.2	_
GZM101	C	84.3	15.7	_

phase according to the selected area electron diffraction (SAED) pattern (Fig. 3(a)). In contrast, except for a few Mg_5Gd particles, large amounts of tiny spherical-shaped particles with the size ~ 20 nm

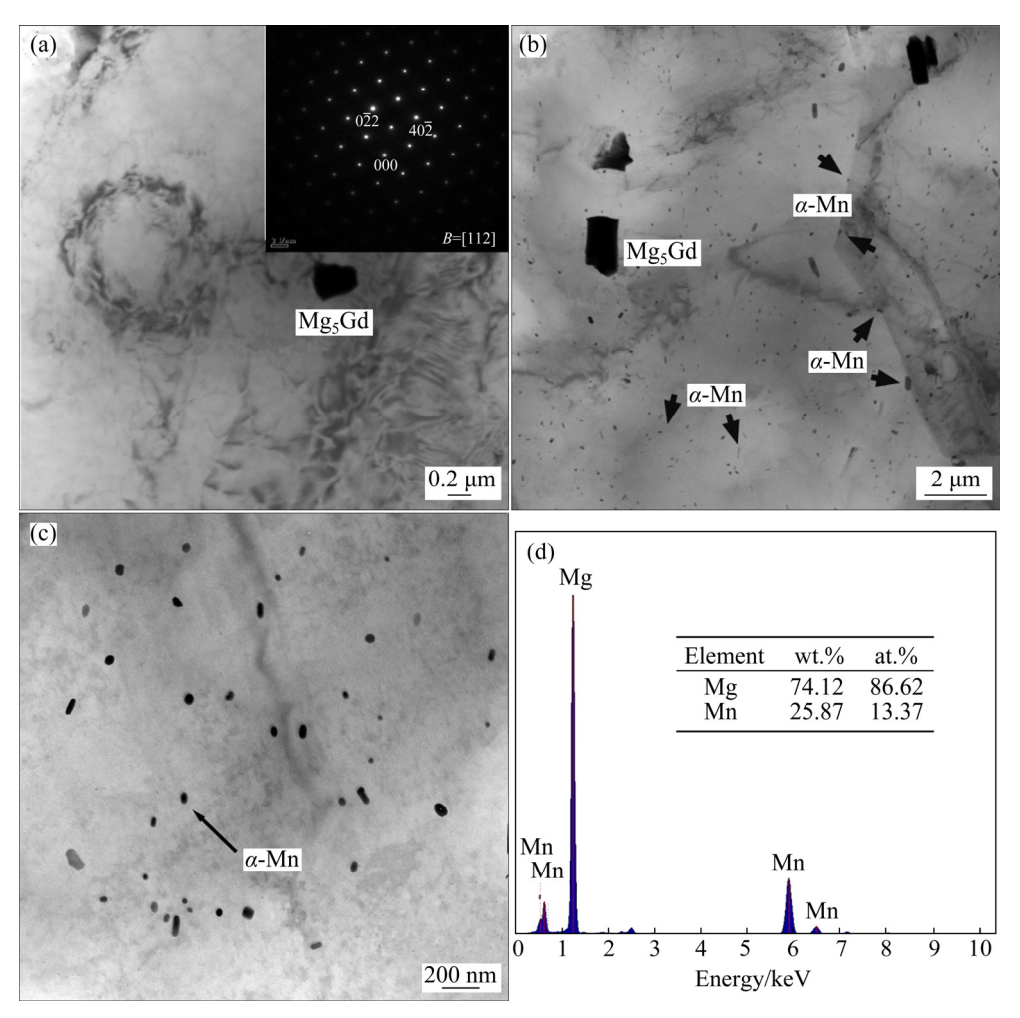


Fig. 3 TEM image and corresponding SAED pattern of particle for extruded GZ10 sheet (a), TEM images (b, c) and EDS results of particles indicated by arrow for GZM101 sheets (d)

also uniformly distribute in the GZM101 sheet (Figs. 3(b, c)). The corresponding EDS results indicate that the spherical-shaped particle is α -Mn particle (Fig. 3(d)).

The inverse pole figure (IPF) mapping, the distribution mapping of grain size and {0001} pole figure of the GZ10–xMn sheets are shown in Fig. 4. These extruded sheets exhibit a completely recrystallized structure. The grain sizes of the extruded GZ10–xMn sheets are decreased with an increment in Mn addition. The mean grain sizes of the GZ10, GZ100 and GZ101 sheets are (18.6±2.1), (16.3±1.6) and (8.6±1.2) μm, respectively. This implies that Mn addition refines the grain size of the Mg alloys [28,29].

The extruded GZ10 sheet shows an ED-split texture, indicated by c-axis of most grains tilting about $\pm 42^{\circ}$ away from the ND towards ED (Fig. 4(a)). With the increase of Mn content, the type of ED-split texture is unchanged, but its

maximum intensity accordingly decreases. The maximum texture intensities of the GZ10, GZ100 and GZ101 sheets are 13.30, 11.84 and 10.47, respectively.

Figure 5 presents the EBSD results of the extruded GZ10-xMn sheets stretched along ED and TD at a tensile strain of 0.1. Some {1012} tension twins (red lines in Fig. 5) are observed in the extruded GZ10-xMn sheets stretched along ED, whereas the amount of tension twins along the TD is less than that along the ED. There are no other twins presented, such as contraction and double twins. It is reported that {1012} tension twinning is considered as one of the main plastic deformation modes due to the low critical resolved shear stress (CRSS) and high accommodate deformation ability in Mg alloys [24]. The fraction of {1012} tension twins of the extruded GZ10-xMn sheets along TD is less compared to that along ED, which is attributed to an ED-split texture.

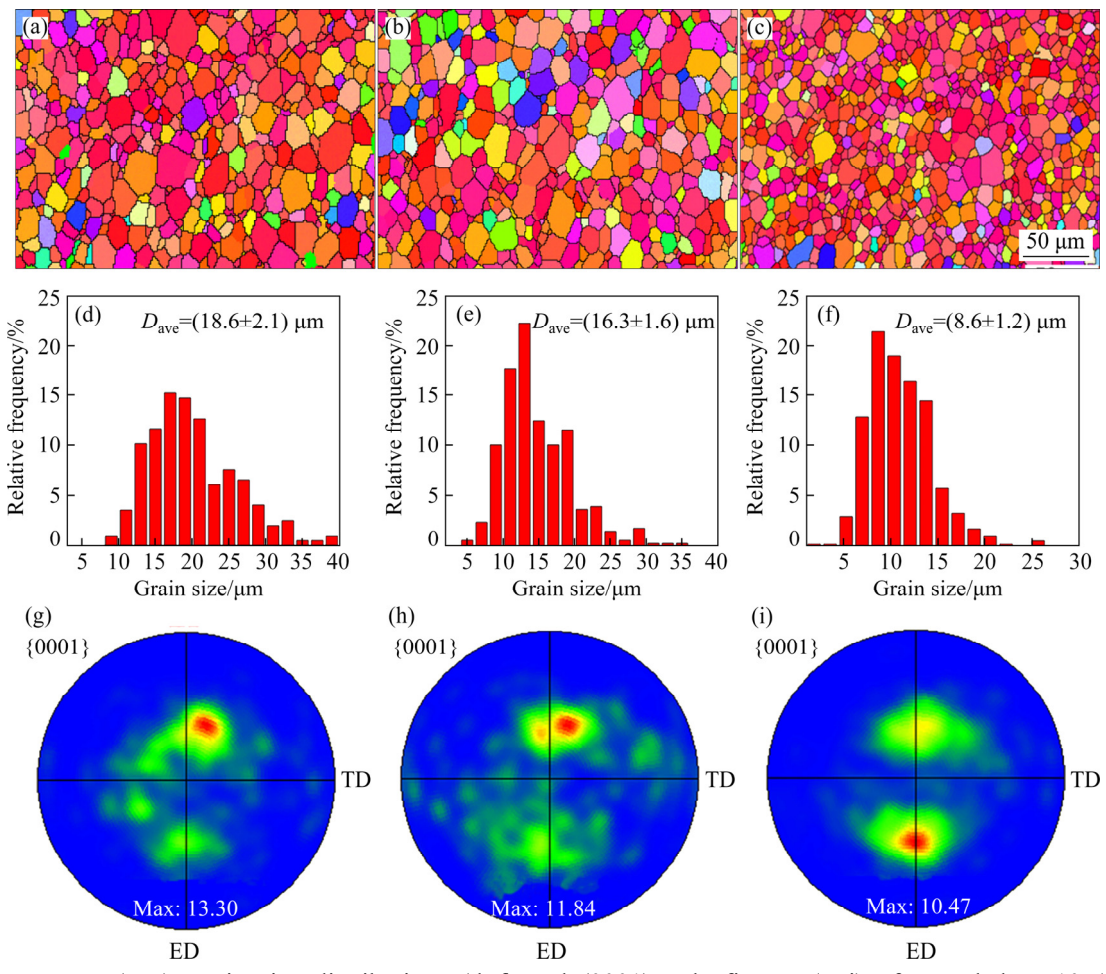


Fig. 4 IPF maps (a-c), grain size distributions (d-f) and (0001) pole figures (g-i) of extruded GZ10 (a, d, g), GZM100 (b, e, h) and GZM101 (c, f, i) sheets

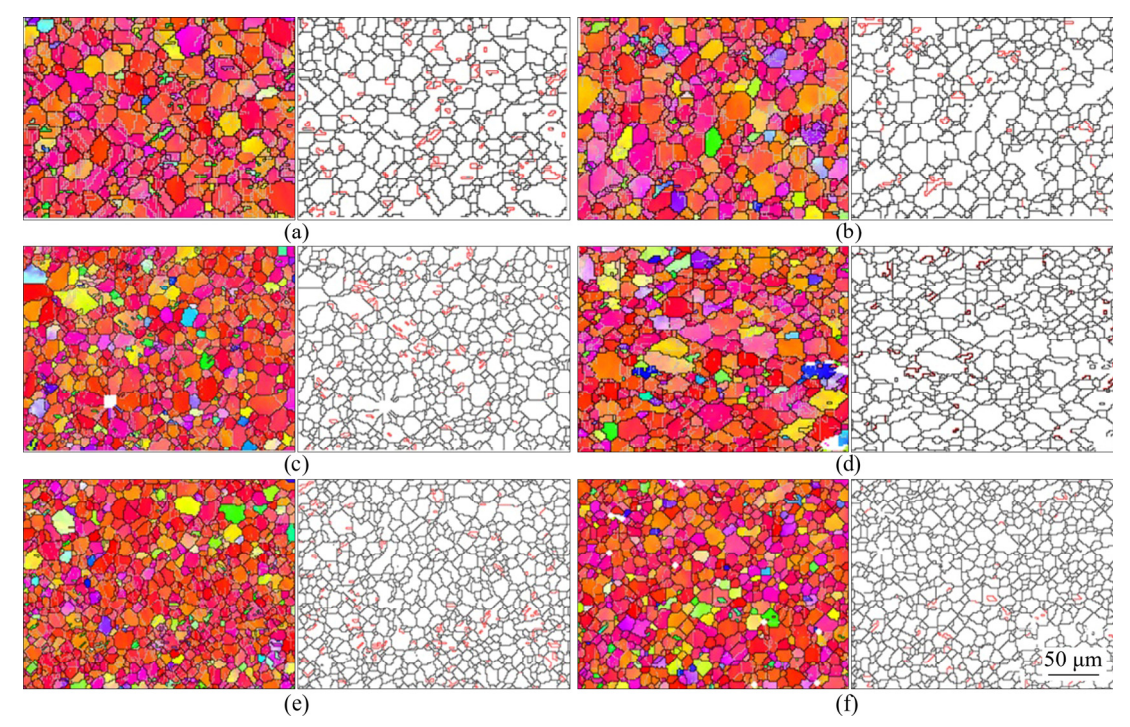


Fig. 5 EBSD results of extruded sheets stretched at tensile strain of 0.1 along ED (a, c, e) and TD (b, d, f): (a, b) GZ10; (c, d) GZM100; (e, f) GZM101

3.2 Mechanical properties

Figures 6(a, b) present the true stress-strain curves of extruded GZ10-xMn sheets stretched along ED and TD, respectively. The main tensile properties are given in Table 2. The yield strength (YS), ultimate tensile strength (UTS) and elongation to failure (EF) of the sheets increase with increasing Mn content, both along ED and TD. The GZM101 sheet exhibits the highest YS, UTS and EF of ~135 MPa, ~352 MPa and ~33.3% along ED, and ~188 MPa, ~333 MPa and ~24.7% along TD, respectively. It is clear that the Mn addition

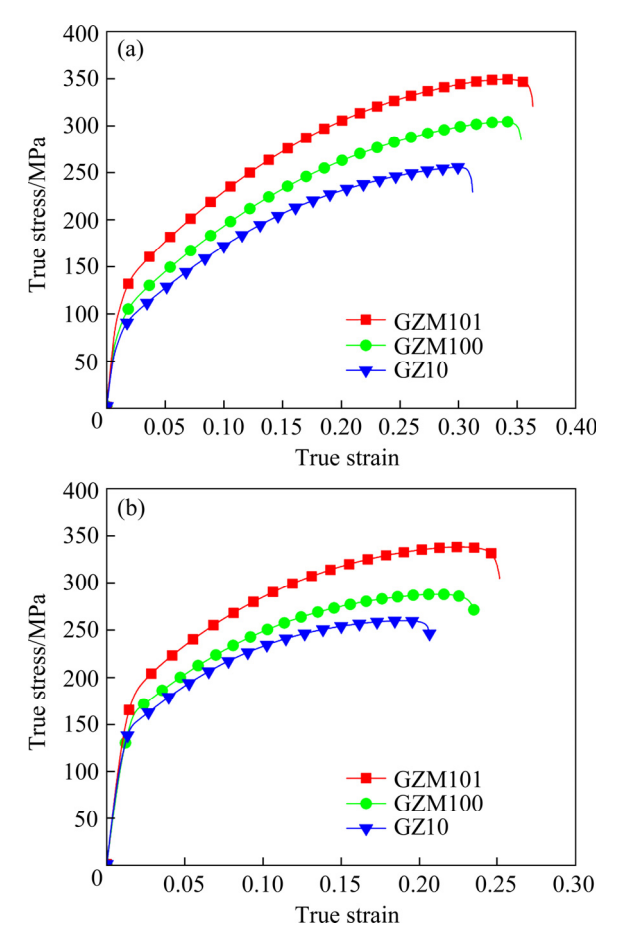


Fig. 6 True stress-strain curves of ED (a) and TD (b) tension of extruded sheets

Table 3 RT tensile properties of extruded sheets

Tensile direction	EF/%	YS/MPa	UTS/MPa
ED	26.5±1.3	83±1.9	254±3.2
TD	17.6±1.6	141±3.2	256±3.6
	26.8±2.1	104±3.6	308±3.1
	22.3±1.4	161±2.9	288±3.7
	33.3±1.5	135±4.1	352±2.9
	24.7±0.8	188±2.8	333±2.7
	ED TD ED TD ED	ED 26.5±1.3 TD 17.6±1.6 ED 26.8±2.1 TD 22.3±1.4 ED 33.3±1.5	TD 17.6±1.6 141±3.2 ED 26.8±2.1 104±3.6 TD 22.3±1.4 161±2.9 ED 33.3±1.5 135±4.1

considerably enhances the tensile properties of the extruded GZ10 sheets.

3.3 Strain hardening behaviour

The strain hardening rate (θ) is employed to study the strain hardening (SH) behaviour of the materials [25]. The θ (d σ /d ε) with (σ - σ _{0.2}) curve is derived from the true stress-strain curve and is shown in Fig. 7, where σ , $\sigma_{0.2}$ and ε are true stress, true YS and true strain, respectively. The θ value drops rapidly at the early deformation stage and then almost linearly decreases, regardless of tensile direction. The hardening capacities (H_c) of the GZ10, GZM100 and GZM101 sheets (H_c= $(\sigma_{\text{UTS}} - \sigma_{0.2})/\sigma_{0.2}$ [26]) are 2.06, 1.96 and 1.61 along ED, and 0.82, 0.78 and 0.77 along TD, respectively (Fig. 8). Further, the Hollomon equation $(\sigma = k\varepsilon^n)$, where n is SH exponent and K is strength coefficient) is used to analyze the SH behaviour. The n value is a key parameter used to assess the strain coordination capacity of Mg alloys [27]. The n value decreases with the increase of Mn content.

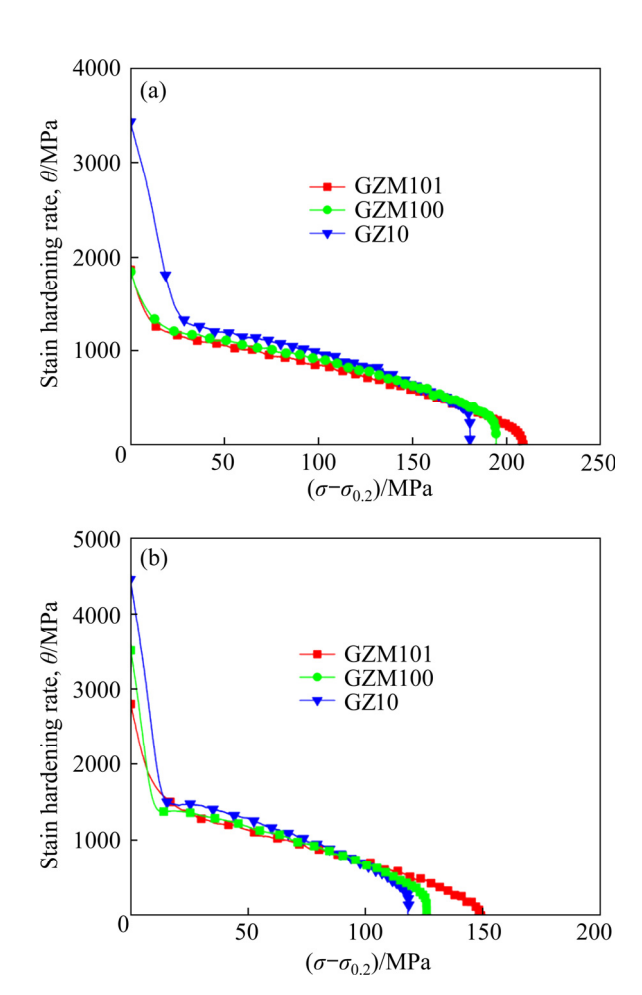


Fig. 7 Strain-hardening rate curves of ED (a) and TD (b) tension of extruded sheets

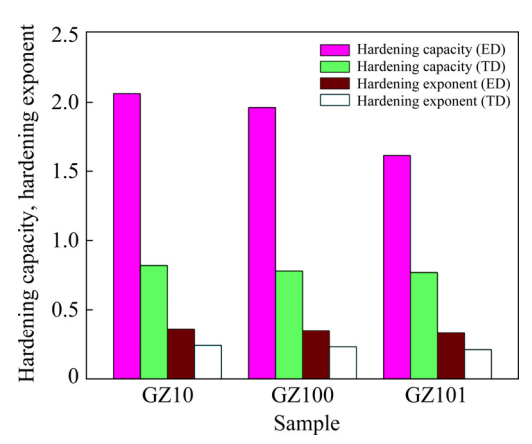


Fig. 8 Hardening capacities and exponents of extruded sheets

The *n* values of the GZ10, GZM100 and GZM101 sheets are calculated to be 0.36, 0.35 and 0.33 along ED, and 0.24, 0.23 and 0.21 along TD, respectively (Fig. 8).

4 Discussion

4.1 Microstructure evolution

Some researchers have reported that the addition of Mn can decrease the grain size of Mg alloys due to the higher number density of α -Mn particles [28,29]. From Fig. 4, the grains of the extruded GZ10 sheet is significantly refined from 18.6 to 8.6 μ m after 1 wt.% Mn addition. It can be inferred that this grain refining mainly results from large amounts of fine α -Mn particles caused by the addition of Mn (Fig. 3(b)) which efficiently impede the movement of grain boundary and hinder the growth of recrystallized grains during extrusion. The relationships of the movement rate of grain boundary and the phase particles are explained by the following equation [30]:

$$V = M_0 \cdot \exp[-Q/(RT)] \cdot (P^{\text{Rex}} - P_z - P_c) \tag{1}$$

$$P_z = 3F_v \cdot \gamma/(2r) \tag{2}$$

where V, M_0 , Q, R, T, P^{Rex} , P_z , P_c , γ , F_v and r are the movement rate of grain boundary, the boundary movement constant, the activation energy, the gas constant, the temperature, the recrystallization driving force, the Zener pressure, the boundary curvature, the shear strain, the fraction and the average radius of the phase particles, respectively. Increasing the fraction of the phase particles leads to the increase in the pinning stress, which can decrease the movement rate of grain boundary.

According to TEM observations (Fig. 3), except for a few Mg₅Gd particles, plentiful and uniform distribution of fine α -Mn particles can be observed in the GZM101 sheet, whereas only a few Mg₅Gd particles present in the GZ10 sheet. Therefore, compared with GZ10 sheet, the grain refinement observed in the GZM101 sheet is closely related to the fine α -Mn particles.

As illustrated in Fig. 4, the addition of Mn weakens the recrystallized texture of the GZ10 alloy. It is well known that the solubility of Mn in the Mg matrix is very low, and the effect of Mn solution can be neglected. Additionally, many researchers suggested that the weakening texture is associated with the phase particles, and these phase particles play a key role in the nucleation and growth of grains [31]. The phase particles can effectively affect the grain size of Mg alloys and contribute to the determination of the recrystallized texture. CHAI et al [3] have also reported that Ce addition results in the formation of many fine second phases, and then significantly restricts the growth of DRXed grains during extrusion, leading to the weakening of texture. In this study, the grain size of the extruded GZ10-xMn decreases with the increase in the amount of of α -Mn particles caused by Mn addition. Figure 9 presents the EBSD results showing grain type images and different grain size images of the extruded GZ10-xMn sheets. Almost fully dynamic recrystallization occurs in all the extruded sheets, which indicates that the DRXed grain fractions of the extruded GZ10-xMn sheets are independent of Mn content. Moreover, it can be seen that the fraction of grains with size <10 µm (with relatively low texture intensity) increases considerably with an increase in Mn content, while the fraction of grains with size >10 µm (with relatively high texture intensity) decreases. It is believed that the weakening of texture after Mn addition can be resulted from the suppression of grain growth by fine α -Mn particles.

4.2 Mechanical properties

As we all known, the grain size, texture, phase particle and solute atom are the primary factors that impact on the mechanical properties of Mg alloys [32]. However, in this study, the effect of the solute atom on the mechanical properties can be ignored due to the low solubility of Mn. The grain size effectively affects the mechanical properties

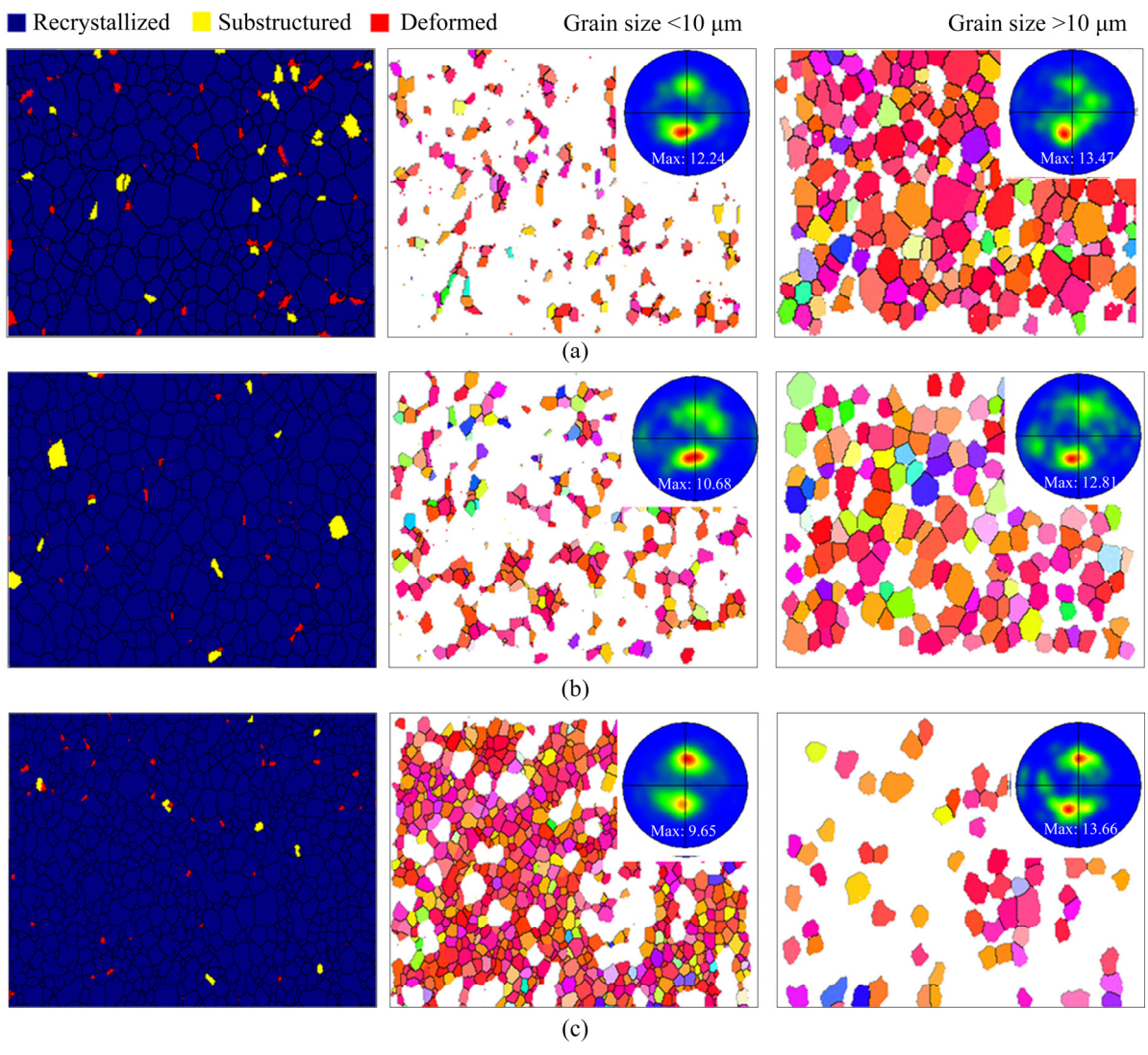


Fig. 9 Different grain types, IPF and {0001} PF maps of extruded sheets with different grain sizes: (a) GZ10; (b) GZM100; (c) GZM101

and grain refinement increases the yield strength [33]. As shown in Fig. 4, the grain sizes of the GZ10-xMn sheets decrease from ~18.6 to ~8.6 µm with increasing Mn addition from 0 to 1 wt.%. According to the Hall-Petch equation:

$$\Delta \sigma_{\text{grain}} = kd^{-1/2} \tag{3}$$

where d and k are the average grain size and HP slope (k=290 MPa· μ m^{1/2} [34]), respectively. The enhancements of the strength for the extruded sheets contributed by the grain size refinement are 67.2, 71.8 and 98.9 MPa for GZ10, GZM100 and GZM101 alloys, respectively. This indicates that grain refining leads to the enhancement of YS. Additionally, the texture can influence the basal $\langle a \rangle$ slip Schmid factor (SF_{basal}) and the YS related to SF_{basal} [35]. The SF_{basal} distributions of the extruded GZ10–xMn sheets stretched along ED and TD are

summarized in Fig. 10. The average SF_{basal} of the extruded sheets slightly increases with Mn addition amount, along both ED and TD. Higher average SF_{basal} exhibits easier basal slip contributing to a reduction for the YS. Further, phase particles play a profound effect on the yield stress of alloys. According to the Orowan equation $(YS \propto f^{1/2} \cdot D^{-1} \cdot \ln D)$ [36], where f and D are the volume fraction and size of phase particles, respectively), increasing volume fraction and decreasing size of phase particles can effectively enhance the YS of the alloys. There are a larger number of fine α -Mn particles formed in the GZM101 sheet, which can significantly restrict the dislocation movement, leading to the increase of YS. Therefore, increasing Mn addition results in the improvement of YS, mainly related to the grain

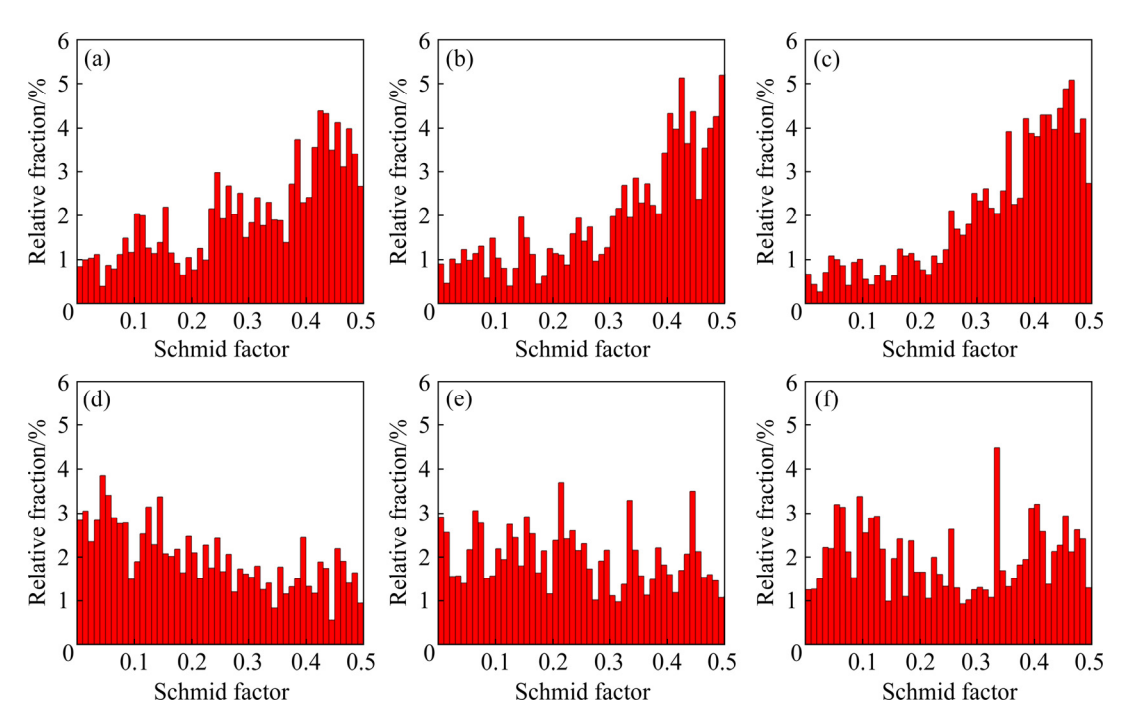


Fig. 10 SF_{basal} distributions of extruded sheets stretched along ED (a–c) and TD (d–f): (a, d) GZ10; (b, e) GZM100; (c, f) GZM101

refining and abundant fine α -Mn particles. In addition, the YS of the sheets in tension along ED is lower than that along TD due to the higher average SF_{basal} and higher activity of tension twins caused by ED-tilted texture (Figs. 5 and 10).

As shown in Fig. 6, the ductility of the extruded GZ10-xMnsheets increases with increasing Mn addition, along both ED and TD. This increase is mainly associated with the grain refining and texture weakening. The grain boundaries play an important role in the coordinate deformation of Mg alloy during the deformation process. Grain refining can increase the grain boundary coordinate ability, which efficiently enhances the ductility of the alloys. In addition, grain refining caused by Mn addition can facilitate the activity of non-basal slip, and thus can improve the ductility of the extruded GZ10 sheet. Also, the addition of Mn results in a slight increase in the average SF_{basal} of extruded GZ10-xMn sheets along ED and TD. Higher average SF_{basal} contribute to easier basal slip activity, and is a way to increase the ductility.

4.3 Strain hardening behaviour

In general, SH behaviour of the metals is controlled by the dislocation migration at the stage

of plastic deformation. Consequently, factors influencing dislocation migration play an essential role in SH behaviour. In Mg alloys, the factors, such as the solute atom, texture and grain size, can effectively affect the SH behaviour [32]. WANG et al [37] reported that solute atoms have a significant effect on SH ability. More solute atoms lead to reducing the dynamic recovery and increasing the dislocation density, which contributes to the enhancement of SH ability. However, the effect of solute atom can be neglected due to the low solubility of Mn in matrix. Besides, texture also affects the slip system activity [33]. During tensile deformation, the angle between the tensile direction and basal pole of grains is $0^{\circ}-45^{\circ}$, and $\{1012\}$ tensile twin and basal slip are easily activated. In contrast, when the angle reaches 90°, {1012} tensile twins and basal slips are hardly activated and prismatic $\langle a \rangle$ slip becomes the primary deformation mode. In this study, basal slip is the primary deformation mode in tension along ED, while prismatic $\langle a \rangle$ slip becomes the primary deformation mode in tension along TD due to the ED-split texture. As given in Table 3, the SF_{basal} increases with increasing Mn addition, both along ED and TD, indicating an increase in basal slip with increasing Mn addition. Previous studies [38]

revealed that increasing basal slip activity results in the decrease in dynamic recovery, leading to the high SH capacity. Therefore, the weakening of texture and the reduction of dynamic recovery can lead to the increase of hardening rate.

However, hardening rates of the extruded GZ10-xMn alloys show a gradual decrease with the increase of Mn content. The dynamic recovery of Stage III is analyzed using $\theta_{\rm III}$ determined by extrapolation to $(\sigma - \sigma_{0.2}) = 0$. From Fig. 7, it can be calculated that the value of $\theta_{\rm III}$ in extruded sheets reduces from 1510 to 1269 MPa along ED, and from 1675 to 1526 MPa along TD. This decrease is mainly due to the grain refinement. DELVALLE et al [33] have reported that grain size effectively influences the SH behaviour and the grain refinement increases the dynamic recovery (the alloys with lower grain size exhibits lower SH capacity). Therefore, a decrease in SH rate with the increase of Mn addition is mainly associated with the grain refinement, which counteracts the enhanced effect from the weakened texture. Moreover, with an increase in Mn content, a reduction in the SH rate results in an increment of EF from 26.5% to 33.3% along ED and from 17.6% to 24.7% along TD. LIAO et al [20] have also revealed that an increase in EF with increment in Mn content results in a decrease of SH.

5 Conclusions

- (1) The grain size of the extruded GZ10–xMn sheets is gradually reduced with increasing Mn addition. This decrease is due to the inhibition of grain growth by fine α -Mn particles. A larger number of fine α -Mn particles are formed and uniformly distribute in the extruded GZM101 sheet to restrain the grain growth. A weak ED-titling texture is formed in all the extruded sheets. There are weak ED-titling textures with Mn addition.
- (2) The strength and ductility of extruded GZ10-xMn sheets increase gradually with an increase in Mn content, mainly associated with fine grain structure caused by fine Mn particles.
- (3) The strain-hardening ability of extruded GZ10-xMn sheet is decreased with increase of Mn addition. The strain-hardening exponent and capacity are gradually reduced with an increment in Mn content. Grain refinement plays an important role in the reduction of strain-hardening ability.

Acknowledgments

The authors are grateful for the National Natural Science Foundation of China (Nos. U1764253, U2037601, 52001037 and 51971044), the National Defense Basic Scientific Research Program of China, the Chongqing Science and Technology Commission, China (No. cstc2017zdcyzdzxX0006), and the Qinghai Science and Technology Program, China (No. 2018- GX-A1).

References

- [1] SONG Yan, YANG Hua-bao, CHAI Yan-fu, WANG Qing-hang, JIANG Bin, WU Liang, ZOU Qin, HUANG Guang-sheng, PAN Fu-sheng, ATRENS A. Corrosion and discharge behavior of Mg–xLa alloys (x=0.0–0.8) as anode materials [J]. Transactions of Nonferrous Metals Society of China, 2021, 31: 1979–1992.
- [2] ZHANG Wan-peng, MA Ming-long, YUAN Jia-wei, SHI Guo-liang, LI Yong-jun, LI Xing-gang, ZHANG Kui. Microstructure and thermophysical properties of Mg-2Zn-xCu alloys [J]. Transactions of Nonferrous Metals Society of China, 2020, 30: 1803–1815.
- [3] CHAI Yan-fu, HE Chao, JIANG Bin, FU Jie, JIANG Zhong-tao, YANG Qin-shan, HUANG Guan-sheng, ZHANG Ding-fei, PAN Fu-sheng. Influence of minor Ce additions on the microstructure and mechanical properties of Mg-1.0Sn-0.6Ca alloy [J]. Journal of Materials Science and Technology, 2020, 37(15): 26-37.
- [4] HOU Cai-hong, YE Zhi-song, QI Fu-gang, WANG Qing, LI Lian-hui, OUYANG Xiao-ping, ZHAO Nie. Effect of Al addition on microstructure and mechanical properties of Mg-Zn-Sn-Mn alloy [J]. Transactions of Nonferrous Metals Society of China, 2021, 31: 1951–1968.
- [5] PAN Shi-wei, XIN Yun-chang, HUANG Guan-jie, LI Qi, GUO Fei-long. Tailoring the texture and mechanical anisotropy of a Mg-2Zn-2Gd plate by varying the rolling path [J]. Materials Science and Engineering A, 2016, 653: 93-98.
- [6] HUA Xun, LV Fei, WANG Qi, DUAN Qin-qin, ZHANG Zhi-fei. Achieving synchronous improvement of strength and ductility of Mg-3%Al-1%Zn alloy through controlling the rolling orientation [J]. Materials Science and Engineering A, 2013, 586: 38-44.
- [7] XU Jun, SONG Jiang-feng, JIANG Bin, HE Jun-jie, WANG Qing-hang, LIU Bo, HUANG Guan-sheng, PAN Fu-sheng. Effect of effective strain gradient on texture and mechanical properties of Mg-3Al-1Zn alloy sheets produced by asymmetric extrusion [J]. Materials Science and Engineering A, 2017, 706: 172-180.
- [8] GU Dong-dong, WANG Jia-wen, CHEN Yu-bin, PENG Jian. Effect of Mn addition and refining process on Fe reduction of Mg-Mn alloys made from magnesium scrap [J]. Transactions of Nonferrous Metals Society of China, 2020, 30: 2941-2951.
- [9] SHI Zhang-zhi, XU Jun-yi, YU Jing, LIU Xue-feng. Microstructure and mechanical properties of as-cast and

- as-hot-rolled novel Mg–xSn–2.5Zn–2Al alloys (*x*=2, 4 wt.%) [J]. Materials Science and Engineering A, 2018, 712: 65–72.
- [10] WANG Yong-jian, PENG Jian, ZHONG Li-ping. On the microstructure and mechanical property of as-extruded Mg-Sn-Zn alloy with Cu addition [J]. Journal of Alloys and Compounds, 2018, 744: 234-242.
- [11] KIM S, PARK S. Underlying mechanisms of drastic reduction in yield asymmetry of extruded Mg-Sn-Zn alloy by Al addition [J]. Materials Science and Engineering A, 2018, 733: 285-290.
- [12] CHANG Li-li, TANG Hong, GUO Jian, Strengthening effect of nano and micro-sized precipitates in the hot-extruded Mg-5Sn-3Zn alloys with Ca addition [J]. Journal of Alloys and Compounds, 2017, 703: 552-559.
- [13] YOU Si-hang, HUANG Yuan-ding, KAINER K, HORT N. Recent research and developments on wrought magnesium alloys [J]. Journal of Magnesium and Alloys, 2017, 5: 239–253.
- [14] WANG Kui, WANG Jing-feng, PENG Xing, GAO Shi-qing, HU Hao, ZENG Lin-jie, PAN Fu-sheng. Microstructure and mechanical properties of Mg-Gd-Y-Zn-Mn alloy sheets processed by large-strain high-efficiency rolling [J]. Materials Science and Engineering A, 2019, 748: 100-107.
- [15] FU Wu, WANG Ru-hao, XUE Hi, KUANG Jing, ZHANG Jin-yu, LIU Guan, SUN Jun. Effects of Zr addition on the multi-scale second-phase particles and fracture behavior for Mg-3Gd-1Zn alloy [J]. Journal of Alloys and Compounds, 2018, 747: 197–210.
- [16] BIAN Li-ping, ZHAO Yuan-liang, ZHOU Yi-chen, WANG Tao, WANG Li-peng, LIANG Wei. Effect of Al–Sr master alloy on the formation of long period stacking ordered phase and mechanical properties of Mg–Gd–Zn alloy [J]. Materials Science and Engineering A, 2018, 738: 125–134.
- [17] WEN Qi, DENG Kun-kun, SHI Ju-yan, ZHANG Bao-ping, LIANG Wei. Effect of Ca addition on the microstructure and tensile properties of Mg-4.0Zn-2.0Gd alloys [J]. Materials Science and Engineering A, 2014, 609: 1-6.
- [18] LI Bai-shun, GUAN Kai, YANG Qiang, NIU Xiao-dong, ZHANG Dong-dong, YU Zi-jian, ZHANG Xu-hu, TANG Zong-min, MENG Jian. Effects of 0.5 wt.% Ce addition on microstructures and mechanical properties of a wrought Mg-8Gd-1.2Zn-0.5Zr alloy [J]. Journal of Alloys and Compounds, 2018, 763: 120-133.
- [19] ZHU Tian-yu, FU Peng-huai, PENG Li-ming, HU Xiao-yu, ZHU Shou-ru, DING Wen-jiang. Effects of Mn addition on the microstructure and mechanical properties of cast Mg-9Al-2Sn (wt.%) alloy [J]. Journal of Magnesium and Alloys, 2014, 2: 27-35.
- [20] LIAO Hong-xin, KIM J, LIU Ting-ting, TANG Ai-tao, SHE Jia, PENG Peng, PAN Fu-sheng. Effects of Mn addition on the microstructures, mechanical properties and workhardening of Mg-1Sn alloy [J]. Materials Science and Engineering A, 2019, 754: 778-785.
- [21] KHAN S, MIYASHITA Y, MUTOH Y, SAJURI Z. Influence of Mn content on mechanical properties and fatigue behavior of extruded Mg alloys [J]. Materials Science and Engineering A, 2006, 420: 315–321.
- [22] LI Z T, QIAO X G, XU C, LIU X Q, KAMADO S, ZHENG M Y. Enhanced strength by precipitate modification in

- wrought Mg-Al-Ca alloy with trace Mn addition [J]. Journal of Alloys and Compounds, 2020, 836: 154689.
- [23] WANG Yi, RONG Wei, WU Yong, PENG Li-ming, CHEN Jie, DING Wen-jiang. Effects of Mn addition on the microstructures and mechanical properties of the Mg-15Gd-1Zn alloy [J]. Journal of Alloys and Compounds, 2017, 698: 1066-1076.
- [24] ZHAO Yang, CHANG Li-li, GUO Jun, JIN Ying. Twinning behavior of hot extruded AZ31 hexagonal prisms during uniaxial compression [J]. Journal of Magnesium and Alloys, 2019, 7: 90–97.
- [25] KOCKS U F, MECKING H. Physics and phenomenology of strain hardening: The FCC case [J]. Progress in Materials Science, 48: 171–273.
- [26] AFRIN N, CHEN D L, CAO X, JAHAZI M. Strain hardening behavior of a friction stir welded magnesium alloy [J]. Scripta Materialia, 2007, 93: 1004–1007.
- [27] ZHANG Zhi-ying, WU Yin, ZHOU Jiao, LIU Xiao-jun, LU Zhao-ping. Strong work-hardening behavior in a Ti-based bulk metallic glass composite [J]. Scripta Materialia, 2013, 69: 73–76.
- [28] YU Zheng-wen, TANG Ai-tao, WANG Qin, GAO Zheng-yuan, HE Jie-jun, SHE Jia, SONG Kai, PAN Fu-sheng. High strength and superior ductility of an ultra-fine grained magnesium—manganese alloy [J]. Materials Science and Engineering A, 2015, 648: 202–207.
- [29] YU Zheng-wen, TANG Ai-tao, HE Jie-jun, GAO Zheng-yuan, SHE Jia, LIU Jian-guo, PAN Fu-sheng. Effect of high content of manganese on microstructure, texture and mechanical properties of magnesium alloy [J]. Materials Characterization, 2018, 136: 310–317.
- [30] HUANG K, MARTHINSEN K, ZHAO Qing-long, LOGÉ R. The double-edge effect of second-phase particles on the recrystallization behaviour and associated mechanical properties of metallic materials [J]. Progress in Materials Science, 2018, 92: 284–359.
- [31] ROBSON J D, HENRY D T, DAVIS B. Particle effects on recrystallization in magnesium-manganese alloys: Particlestimulated nucleation [J]. Acta Materialia, 2009, 57: 2739–2747.
- [32] ZHAO Chao-yue, CHEN Xian-hua, PAN Fu-sheng, GAO Shang-yu, ZHAO Di. Effect of Sn content on strain hardening behavior of as-extruded Mg-Sn alloys [J]. Materials Science and Engineering A, 2018, 713: 244-252.
- [33] DELVALLE J A, CARRENO F, RUANO O A. Influence of texture and grain size on work hardening and ductility in magnesium-based alloys processed by ECAP and rolling [J]. Acta Materialia, 2006, 54: 4247–4259.
- [34] YU Hui-hui, LI Chang-zheng, XIN Yun-chang, CHAPUIS A, HUANG Xiao-xu, LIU Qin. The mechanism for the high dependence of the Hall-Petch slope for twinning/slip on texture in Mg alloys [J]. Acta Materialia, 2017, 128: 313-326.
- [35] JIANG M G, XU C, NAKATA T, YAN H, CHEN R S, KAMADO S. Rare earth texture and improved ductility in a Mg-Zn-Gd alloy after high-speed extrusion [J]. Materials Science and Engineering A, 2016, 667: 233-239.
- [36] NIE Jian-feng. Effects of precipitate shape and orientation on dispersion strengthening in magnesium alloys [J]. Scripta

Materialia, 2003, 48: 1009-1015.

- [37] WANG Hui-yuan, RONG Jian, LIU Guo-jun, ZHA Min, JIANG Qi-chuan. Effects of Zn on the microstructure and tensile properties of as-extruded Mg-8Al-2Sn alloy [J]. Materials Science and Engineering A, 2017, 698: 249-255.
- [38] SONG Bo, HUANG Guan-sheng, LI He, ZHANG Lei, PAN Fu-sheng. Texture evolution and mechanical properties of AZ31B magnesium alloy sheets processed by repeated unidirectional bending [J]. Journal of Alloys and Compounds, 2010, 489: 475–481.

Mn 的添加协同提升挤压态 Mg-Gd-Zn 合金强度与塑性

赵 俊1, 蒋 斌2, 宋 燕2, 戴作财1, 卢立伟3, 何 超2, 黄光胜2, 张丁非2, 潘复生2

- 1. 湖南城市学院 机械与电气工程学院, 益阳 413002;
- 2. 重庆大学 材料科学与工程学院 机械传动国家重点实验室, 重庆 400044;
 - 3. 湖南科技大学 材料科学与工程学院,湘潭 411201

摘 要:采用 X 射线衍射仪(XRD)、扫描电子显微镜(SEM)和背散射电子衍射仪(EBSD)研究 Mn 含量对挤压 Mg-1Gd-0.5Zn-xMn (x=0、0.3 和 1,质量分数,%)合金板材显微组织、拉伸性能和应变硬化行为的影响。结果 表明,所有挤压板材均呈现出完全再结晶晶粒组织和向挤压方向偏转的织构。随着 Mn 含量的增加,挤压板材的 平均晶粒尺寸逐渐减小,偏转织构减弱,这主要是由于 Mn 的添加形成新的细小 α -Mn 颗粒相。 拉伸性能结果表明,Mn 的添加提高挤压 Mg-1Gd-0.5Zn-xMn 合金板材的屈服强度、抗拉强度和伸长率,这主要是由于细小的晶粒和 α -Mn 颗粒。 此外,Mg-1Gd-0.5Zn-xMn 合金板材中,Mg-1Gd-0.5Zn-1Mn 合金板材具有最低的应变硬化指数和最好硬化能力。

关键词: Mg-Gd-Zn 合金; Mn 添加; 显微组织; 力学性能

(Edited by Bing YANG)